$$A = \frac{1}{4}\varepsilon_0 \Delta V \frac{\overline{\left(\int \boldsymbol{E}^{old} \times \overline{\mathbf{H}_m} \cdot d\mathbf{S} + \int \overline{\mathbf{E}_m} \times \boldsymbol{H}^{old} \cdot d\mathbf{S}\right)}}{\int Re\left(\boldsymbol{E}_m \times \overline{\mathbf{H}_m}\right) \cdot d\mathbf{S}} \tag{9}$$

where $\overline{\overline{\boldsymbol{G}^{EM}}}(x, x')$ is the electromagnetic Green's function expressing the electric field at x due to a magnetic dipole at x'.

The adjoint simulation described Eq. (8) consists of sending the desired mode backwards into the splitter. This is analogous to Eq. (6), where the adjoint source was located at the measurement point of the Figure-of-Merit. This source problem can be solved with a standard Maxwell solver. FDTD is perfectly suited for this propagating wave problem. Also analogous to Eq (6) the phase of the adjoint source is set using $\boldsymbol{E}^{old}$ and $\boldsymbol{H}^{old}$, from the forward simulation, as described in Eq (9). Once the adjoint simulation is performed, the derivative of the Figure-of-Merit with respect to dielectric permittivity at *every* point in the design region is calculated by combining the forward and adjoint simulations results into Eq. (5). FDTD is perfectly suited to solve the direct and adjoint problem, which consists of propagating waves in a dielectric.

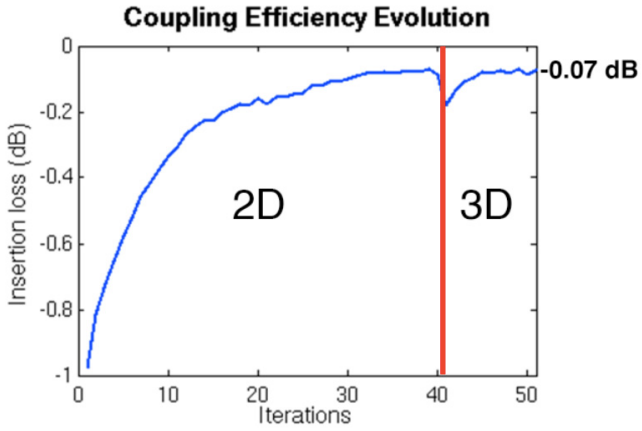

Fig. 3. Coupling efficiency evolution during the optimization. The switch from 2d to 3d FDTD is visible at iteration 41. For comparison, the previous record of ref [3]. was –0.13dB and required 1500 simulations.

This derivative is then used to modify the geometry of the splitter. Since we employed a level set description of geometry, the derivative is used as a velocity field to modify the level set shape. This has the effect of pushing out the geometry boundary when the derivative is positive and pushing it in when it is negative. Since the refractive index if Silicon is higher than that of Silicon dioxide this implements the imperative of the derivative at every point: The Figure-of-Merit benefits from an increase in the dielectric permittivity where the derivative is positive and vice-versa. The step-size criterion for each iteration is a fixed area of changing type in 2d, and a fixed volume in 3d.

The device was first optimized using 2d finite difference time domain (FDTD) simulations of a structure extruded infinitely in the 3rd dimension. In 2d, the effective index method is used and the Silicon is assigned the fictitious refractive index = 2.8, which mimics the proper in-plane wavevector of the correct 3d mode. Once iterative progress stopped in 2d (41 iterations), the problem was transferred to 3d for more iterations. Naturally the first 3d iteration is not as good as the optimized 2d device, since the effective index method is only an approximation. The optimal structure was computed within 51 iterations (102 simulations), achieving a record low insertion loss –0.07dB. By comparison, ref [3]. achieved a minimal

insertion loss –0.13dB, after 1500 simulations using particle swarm optimization. (Note that for such small attenuation, the simulation results are very sensitive to the simulation parameters, which may not have been perfectly identical to ref [3].).

Thus adjoint steepest descent, with much lower computational cost, can yield as good or better results than particle swarm optimizations, which take no advantage of the underlying Maxwell equation physics.

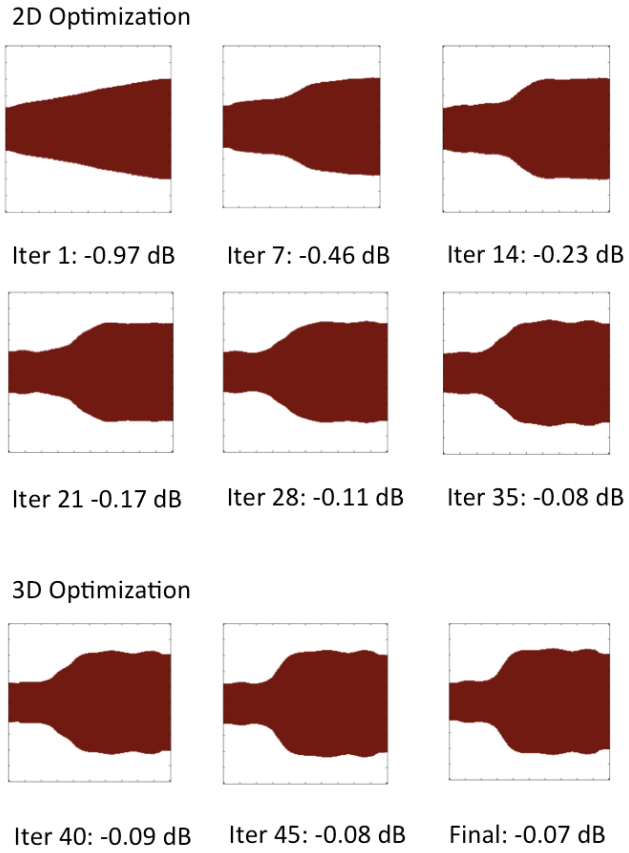

Fig. 4. Geometry evolution during the optimization process and total coupling efficiency to the output waveguides. Iter indicates the iteration number, and the insertion loss is given in dB. The optimization is first carried out using a 2d approximation with an effective waveguide index = 2.8, which mimics the 3d in-plane propagation constant. The final iterative steps are carried out in full 3d FDTD.

The figure of merit evolution, as well as intermediate optimization steps, is presented in Figs. 3. and 4 respectively. There is a visible change between the 2d solution and the 3d solution, with a non-negligible efficiency improvement. This 3d improvement was only possible with the adjoint method, as the 3d computational cost limits the multiple simulations in particle swarm methods. The electric field intensity distribution of the final iteration is shown in Fig. 5. The large operating bandwidth of the optimized structure is shown in Fig. 6. and is good indication of the robustness of the design generated by the optimization.

#194605 - $15.00 USD Received 26 Jul 2013; revised 19 Aug 2013; accepted 20 Aug 2013; published 6 Sep 2013

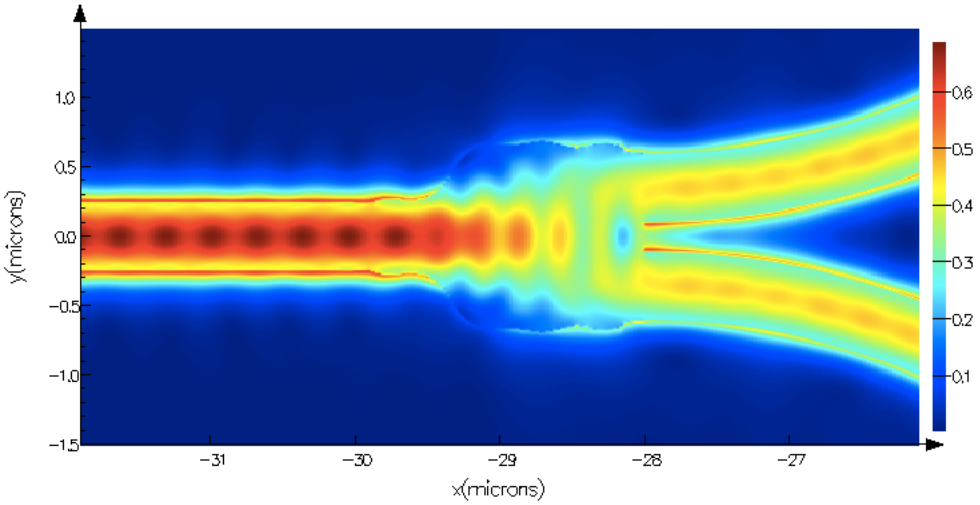

Fig. 5. Simulated field intensity $|\boldsymbol{E}|^2$ for the optimized structure at $\lambda = 1550$nm for a slice in the middle of the device.

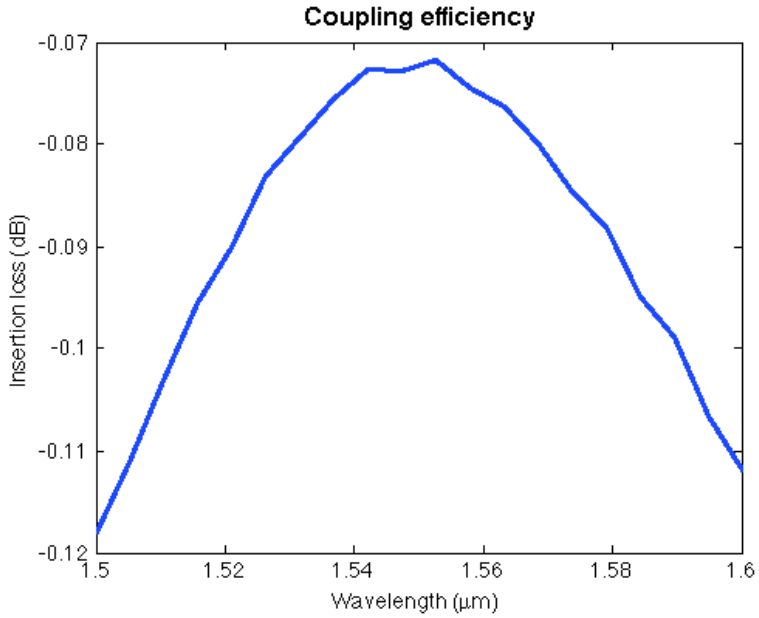

Fig. 6. Simulated insertion loss of the optimized device for wavelengths between 1.5 and 1.6 μm. The broad operating spectrum of the device is a good indicator of the robustness of the design.

4. Conclusion

As photonic and wireless components become an increasingly important part of electronics, it is evident that many problems will require electromagnetic optimization. The computational cost of solving Maxwell's equations is significant, and inefficient design optimization algorithms will become unacceptable. We have shown that the adjoint gradient decent method for shape optimization of sub-wavelength photonic devices can be readily implemented by embedding commercial Maxwell solvers within an inverse optimization algorithm.

#194605 - $15.00 USD Received 26 Jul 2013; revised 19 Aug 2013; accepted 20 Aug 2013; published 6 Sep 2013

For exploration of larger solution spaces where local optima may exist, this method may be augmented with a clever choice of Figure-of-Merit, as well as global optimization routines such as simulated annealing to provide efficient and powerful automated design of photonic components.

Adjoint-gradient-steepest-descent has already beaten the previous record for a manufacturable splitter within current Silicon photonics technology, at much less computational cost than previous methods. This opens the pathway to a more systematic, efficient, photonic component design optimization. The code used for this optimization is available at [21].

Acknowledgments

This work is supported by the Defense Advanced Research Projects Agency (DARPA) E-PHI program under Grant No. HR0011-11-2-0021, the NSF E3S Center under NSF award 0939514, and the U.S. Department of Energy "Light–Material Interactions in Energy Conversion" Energy Frontier Research Center under Grant DE-SC0001293